Challenges for 5G and Beyond*

Jelena Senic[1], Anmol Bhardwaj[1], Camillo Gentile[1], Derek Caudill[2], Chiehping Lai[1], Damir Senic[3], Sung Yun Jun[2], Jack Chuang[1], Jian Wang[1], Anuraag Bodi[1], Raied Caromi[1], Nada Golmie[1]
[1] Wireless Networks Division, National Institute of Standards and Technology, Gaithersburg, MD, USA, jelena.senic@nist.gov
[2] RF Technology Division, National Institute of Standards and Technology, Boulder, CO, USA
[3] Ansys, Inc., Canonsburg, PA, USA

***Abstract*—In this paper, we discuss some challenges for 5G-and-beyond communications systems based on our measurements conducted with millimeter-wave (mmWave) channel sounders. One study analyzes path loss at 28 GHz vs. 83 GHz and in line-of-sight conditions vs. non-line-of-sight conditions and finds it to depend much more heavily on the latter than the former. A significant factor of path loss is penetration loss; in fact, another study focuses on obstructions that are typical in wireless environments: building walls, human bodies, and trees. Finally, in addition to investigating how power is distributed over distance through path loss, we also investigate how power is distributed over delay and angle per distance, otherwise referred to as channel dispersion. In particular, we discuss the importance of diffuse multipath to the total received power at mmWave and the foregone conclusion of wide-sense stationarity, which we show will often not apply to mmWave small-scale fading.**

***Index Terms*—5G, millimeter-wave, mmWave, path loss, penetration loss, sparsity, diffuse components, wide-sense stationarity**

I. Introduction

Wireless providers are exploring the millimeter-wave (mmWave) and sub-Terahertz bands for the deployment of 5G and beyond, what we refer to collectively as next generation systems (*NextG*). NextG will provide multi-Gb/s data rates and latency less than 1 ms, and according to [1] more than half billion 5G subscriptions are expected by the end of 2021 and 3.5 billion by 2026. While higher frequencies offer large swaths of bandwidth to support such strenuous data requirements and the exponential rise in wireless connections, propagation characteristics at mmWave differ significantly from sub-6-GHz bands, where 4G cellular systems currently operate [2-3].

To understand these characteristics and for the development of realistic and reliable channel models, measurements are essential. To that end, we designed our own channel sounders in the 28, 60, and 83 GHz frequency bands [4-5] and conducted numerous measurement campaigns over the past six years in indoor and outdoor environments. In addition, we conducted measurements with the Terragraph[1] 60 GHz phased-array channel sounder [6]. In Section II, we report on path loss measurements, comparing 28 GHz vs. 83 GHz and line-of-sight (LoS) vs. non-line-of-sight (NLoS) conditions. Penetration loss due to indoor and outdoor walls, human bodies, and trees at 60 GHz is discussed in Section III. Finally, Section IV discusses the importance of diffuse components at mmWave and the non-wide-sense stationarity of mmWave small-scale fading. The last section is reserved for conclusions.

[1] Mentioning this product does not imply an endorsement by NIST, but serves to clarify the equipment used.

II. Frequency-Dependent Path Loss

Our first study investigates the frequency-dependent behavior of path loss at 28 GHz and 83 GHz. Measurement campaigns were conducted in a hallway environment in both LoS and NLoS conditions (Fig. 1(a)). The measurement environment represented a hotspot scenario where the transmitter (TX) was fixed at 2.5 m and the receiver (RX) was lower, at 1.6 m. Fig. 1(b) illustrates the path loss results obtained from measurements, where the 28 GHz data is represented by red circles and the 83 GHz data by blue circles. The path-loss model (red and blue solid lines, respectively) was fit to the measured data points through least-squares regression. Free-Space (FS) models predicted from Friis transmission equation [7] for both bands are shown as dashed lines.

In LoS conditions, the path-loss exponent is less than 2.0 (FS exponent), which is common in rich multipath environments due to the coherent summation of the paths. As such, we can still detect signals at the end of the hallway, at 160 m. However, mmWave signals cannot penetrate through the stone wall – what creates NLoS conditions at the "Corner" in Fig. 1(a) – and so they must instead rely on reflected paths, since diffraction at mmWave is so weak [8].

As a result, path loss is much more severe in NLoS: the solid circles represent measured data points while lines with circles denote the fit model. It is interesting to observe that the path loss at 160 m in LoS is still lower than the path loss at 24 m in NLoS. In fact, using a realistic link budget based on New Radio [9], assuming TX power = 38 dBm at 28 GHz and 43 dBm at 83 GHz, TX antenna gain = 17 dBi, RX antenna gain = 0 dBi, bandwidth = 100 MHz to compute noise floor, etc., our models predict that a system operating at 28 GHz can sustain a link distance of 930 m in LoS but only 37 m in NLoS, and in contrast a system operating at 83 GHz can sustain 950 m in LoS but only 25 m in NLoS. In fact, we found that at mmWave propagation depends much less on the center frequency than on the condition, where the path-loss exponent is 1.5 and 1.4 in LoS at 28 GHz and

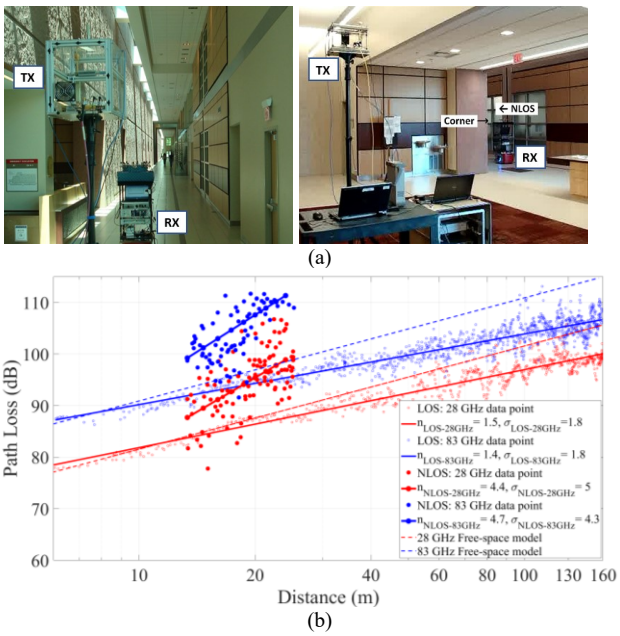

Fig. 1. (a) 28 GHz channel sounder systems in LoS (left) and 83 GHz channel sounder in NLoS created by the "Corner" (right). (b) Measured path loss data points and model fits in LoS and NLoS conditions at 28 GHz (red points and lines) and 83 GHz (blue points and lines).

83 GHz, respectively, and 4.4 and 4.7 in NLoS. The path loss results presented here have been incorporated in Table 2 of Recommendation ITU-R P.1238-11 [10].

III. Penetration Loss

There are a number of factors that contribute to the path loss measured above, namely free-space, oxygen absorption, and penetration losses. As demonstrated through our measurements, free-space path loss can be reliably predicted through Friis transmission equation. Also, oxygen-absorption loss at 60 GHz, where it is most significant in the mmWave band, has also been accurately characterized at about 15 dB/km [2]. So, in this section we focus our efforts on characterizing the penetration loss of typical obstructors, through controlled experiments at 60 GHz.

A. Building Walls

Our study reported in [11] presents measurements for penetration loss at 60 GHz over a variety of the building materials in indoor-to-indoor (I2I) and outdoor-to-indoor (O2I) mobile scenarios. The goal of this study is to capture what a real communications system would experience in the presence of mobility, as opposed to a collection at stationary positions [12-13]. Therefore, the penetration loss was measured across continuous incident points and at different incident angles along the surface of the building materials in the environment. During the measurements, the TX was first placed in an office (I2I scenario) and then outside of a building (O2I scenario), while the RX was mounted on a mobile robot that moved along an interior hallway. The penetration loss strongly depends on the material: the

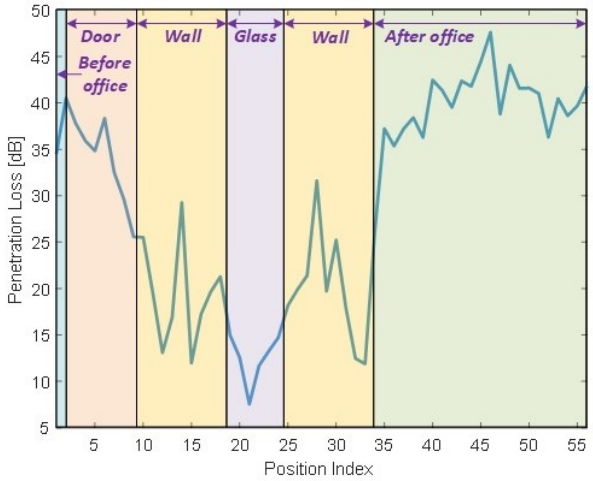

Fig. 2. Measured penetration loss for indoor-to-indoor scenario [11].

wooden door, plasterboard wall, and interior glass were observed to have loss up to 40.5 dB, 31.6 dB, and 18.1 dB, respectively (Fig. 2), while the exterior building materials exhibited even larger penetration losses, up to 66.5 dB.

B. Human Body

NIST conducted an extensive measurement campaign at 60 GHz with three human subjects, to investigate the effect of human blockage at mmWave [14]. The TX and RX were fixed at the same height of 1.6 m, with separate distance between them varying from 4 m to 8 m. Each person traversed a linear trajectory perpendicular to the LoS path at a walking speed of about 0.3 m/s. A total of 1500 measurements were captured within an interval of 5.1 s per scenario, with the shadowing falling in the middle of the interval. Measured signal profiles during a shadowing event with three human subjects are shown in Fig. 3. The maximum shadowing gain ranged from 12.1 dB to 26.1 dB, depending on the body shape and height.

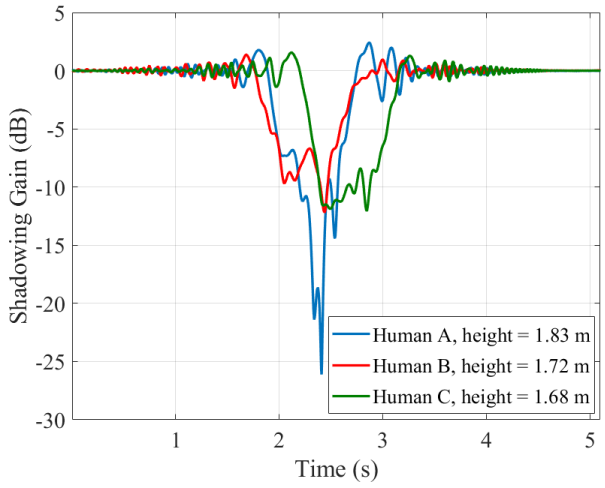

Fig. 3. Measured signal profile during shadowing event for three human subjects with different body structures and heights.

C. Trees

The penetration loss of trees is another important factor that must be considered at mmWave, given their pervasiveness outdoors. We found that the degree of attenuation depends both on the tree type and on the vegetation density, the latter changing with seasons. To explore the seasonal effects on channel propagation through trees, NIST conducted measurement campaigns in summer and winter on several tree types at 60 GHz. Measurements were collected at 14 distinct RX locations around each tree for a fixed TX position, and for different TX-RX beam combinations, collecting nearly 25,000 channel measurements per tree. The TX and RX antennas were positioned at the same height of 4.6 m with the antennas facing each other. The LoS was obstructed by the tree trunk, branches, and leaves, where the diameter of the tree crown varied between 5 m to 12 m depending on the tree type. In addition to the measurements, propagation simulations were run using ANSYS HFSS SBR+ (High Frequency Structure Simulator Shout and Bounce Ray)[2] software on the CAD (Computer Aided Design) models of the trees, both for validation and tuning.

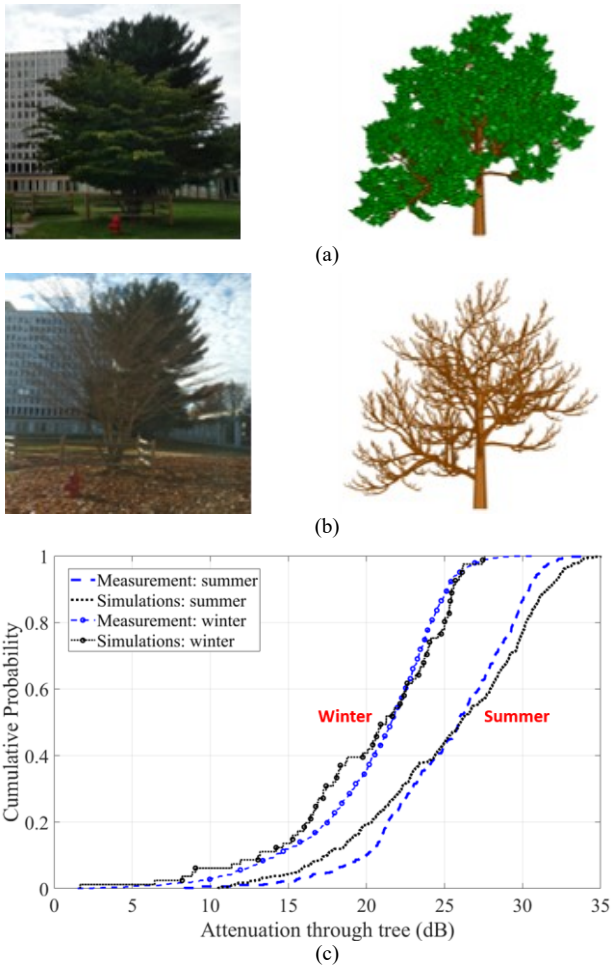

Fig. 4. (a) Photograph of European Nettle tree measured on NIST Gaithersburg campus (left) and realistic CAD model of the tree used in ANSYS HFSS software (right) for the summer scenario. (b) The same tree during winter after the leaves withered. (c) Cumulative distribution functions for the attenuation through this tree with rich vegetation in summer (lines with no symbols) and poor vegetation during winter (lines with symbols); dashed blue lines indicate measured data while dotted black lines indicate simulated data.

Fig. 4(a) shows a photograph (left) of a measured tree (European Nettle) in summer and its realistic CAD model (right). This is followed by the same tree in winter, after the leaves had withered (Fig. 4(b)). Cumulative distribution functions (CDFs) for the attenuation through this tree with rich vegetation in summer (lines with no symbols) and poor vegetation in winter (lines with symbols) are presented in Fig. 4(c), where the dashed blue lines indicate the measured data and the dotted black lines indicate the simulated data. The average (50% on CDFs) attenuation in summer was 27.1 dB, but relaxed to 22.2 dB in winter. Statistics on the attenuation through trees were reduced from the measurements and contributed to the Recommendation ITU-R P.833-10 under section titled "Seasonal effects on single trees at 60.5 GHz" [15].

IV. Channel Dispersion

The two previous sections concentrated on path loss at mmWave, *i.e.*, the distribution of the received power over distance. In this section, we concentrate on the distribution of the received power in delay and angle *per distance*, what is referred to as *channel dispersion*. In particular, we discuss the importance of diffuse power at mmWave and the non-wide-sense stationarity of the channel.

A. Diffuse Power

Thanks to negligible diffraction at mmWave [8], the majority of the received power can be attributed to the LoS path (when present) and to specular reflections. As there are just a few dominant paths, the mmWave channel is often referred to as *sparse*. Yet, the misconception in many papers is that the mmWave channel can be accurately represented by just the dominant paths. In reality, diffuse components, which appear only when the wavelength is comparable to the dimensions of the scatterers, *i.e.*, at mmWave, can account for up to 40% of the power [16]. In fact, Fig. 5 illustrates the dispersion of the measured paths in the angle and delay domains in a lecture room environment at 60 GHz. As can be observed, there are hundreds of paths – not just a few – and the diffuse paths tend to cluster around the specular paths, forming clusters, labeled in the legend against the main scatterers in the environment that generated the clusters [17]. Note that even third order reflections can be identified. From this figure, we calculated the percentage of specular and diffuse power in each cluster. See Table I. We can observe that diffuse power can account for as high as 46.6% of the total power per cluster (*Left wall* scatterer).

So, when transceivers steer their beams toward specular paths, they will detect diffuse paths as well. While the diffuse power will in general increase the amount of received

[2] Mentioning this product does not imply an endorsement by NIST, but serves to clarify the software used.

TABLE I
DISTRIBUTION IN POWER OF SPECULAR COMPONENTS WITH RESPECT TO THE DIFFUSE COMPONENTS FOR DIFFERENT SCATTERERS IN THE LECTURE ROOM

	Ceil.	Right wall	Glass door	Right + Left	Left wall	Proj.	Cor. 1	Cor. 2	Top wall	Left + Right	Glass + Right	Left + Top	Glass + Cor. 1	Left + Right + Left	Right + Left + Right
Specular Power (%)	66.6	82.7	84.4	93.2	53.4	68.5	84.9	60.2	73.3	84.9	81.2	81	79.9	82.2	82.3
Diffuse Power (%)	33.4	17.3	15.6	6.8	46.6	31.5	15.1	39.8	26.7	15.1	18.8	19	20.1	17.8	17.7

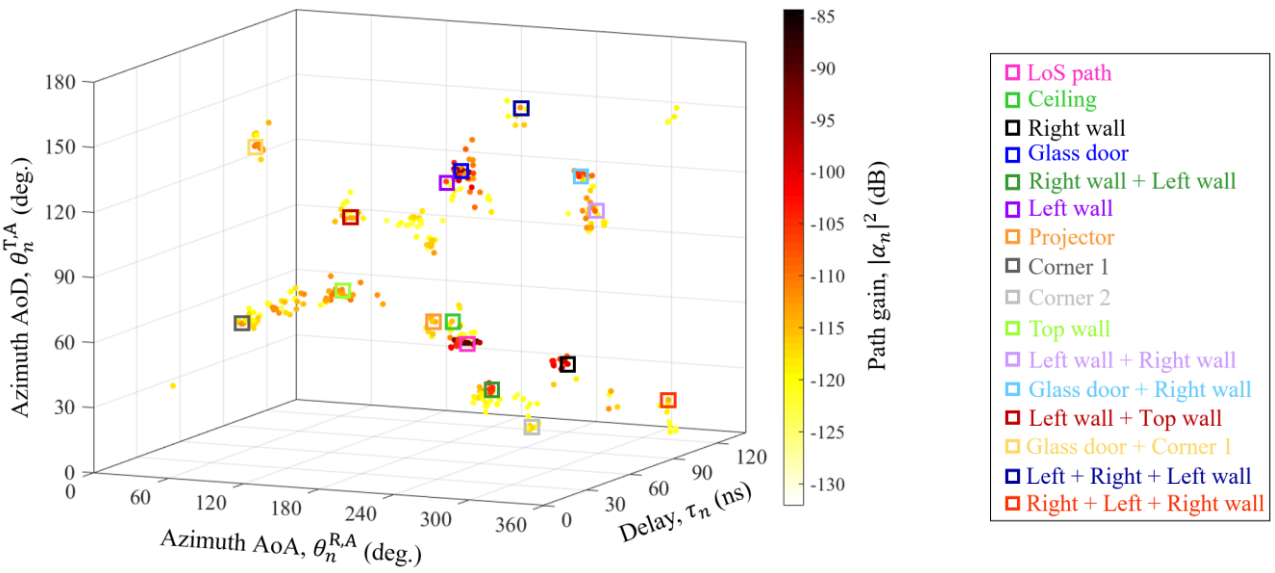

Fig. 5. Measured channel paths in the lecture room displayed in the azimuth angle-of-departure (AoD) vs. azimuth angle-of-arrival (AoA) vs. delay and color-coded against path gain in the colorbar [17]. The specular path of each cluster identified is marked with a square that is color-coded in the legend against the scatterer that generated the cluster. The weaker diffuse components tend to cluster around the specular one.

power so that longer link distances can be sustained, they will also give a rise to fading, as the paths will interfere with each other, generating small-scale fading when in motion, as we shall see in the sequel.

B. Non-Wide-Sense Stationarity

The *coherence time* in wireless channels intends the time over which a signal does not change appreciably due to fading that arises from multipath effects only, that is, the coherent summation of paths with similar amplitudes but random phases. This sort of fading is referred to as *small-scale* or *fast* and is witnessed in rich, omnidirectional, wideband scattering environments, resulting in a channel that is said *wide-sense stationary* (WSS), meaning that its second-order statistics, *i.e.*, its mean and variance, are constant over time. While WSS holds for sub-6 GHz systems, our recent measurements in [18] confirmed that WSS assumption may not hold for mmWave, not only because the channel is sparse, but also because the highly directional antennas will detect just a few paths. What's more, since bandwidths will be on the order of hundreds – rather than tens – of MHz, the receiver will be able to detect individual paths rather than their coherent summation, so less small-scale fading will be experienced altogether.

To quantify the WSS vs. non-WSS conditions, we employed the Augmented Dickey-Fuller (ADF) test [19]. The ADF test checks for a unit root in a time series sample, where the existence of a unit root means that its second-order statistics are not constant. Figures 6(a) and 6(b) show the ADF test statistic as a function of increasing beamwidth[3] and decreasing bandwidth[4]. The critical values (CV) are shown as the orange line in both plots. When the ADF test statistic is greater than CV, the channel is non-WSS. We can see that the channel becomes WSS for beamwidths in excess of about 45° and for bandwidths less than about 1 GHz.

[3] For fixed 2 GHz bandwidth.
[4] For omnidirectional beamwidth.

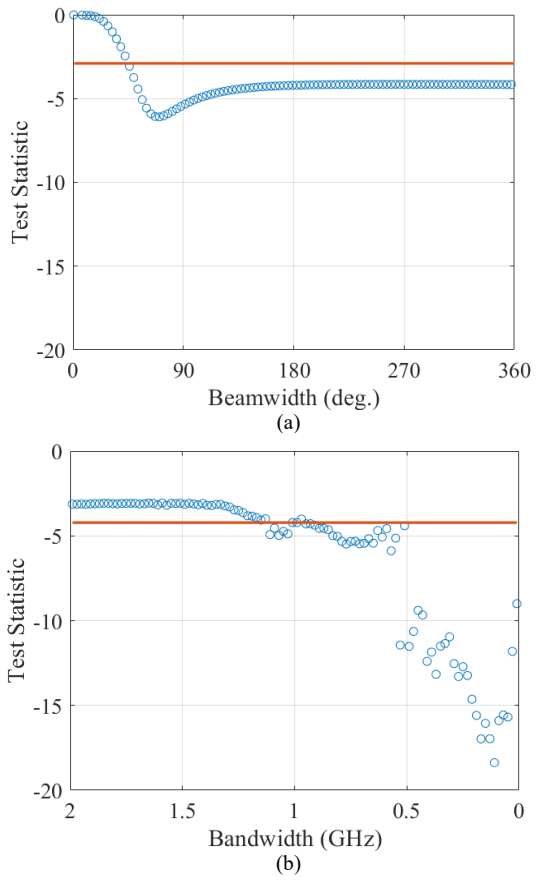

Fig. 6. (a) Augmented Dickey-Fuller (ADF) test statistic as a function of increasing beamwidth. (b) ADF test statistic as a function of decreasing bandwidth. Critical Value (CV) is indicated using the orange line in both cases. Test statistic greater than CV implies non-wide-sense stationary channel. Test statistic less than CV implies wide-sense stationary channel.

V. Conclusion

In this paper, we reported findings on mmWave propagation based on measurements collected with 28, 60, and 83 GHz channel sounders. While the path loss in LoS can readily sustain link distances up to 930 m and 950 m at 28 GHz and 83 GHz respectively, in NLoS the corresponding link distances dropped to just 37 m and 25 m. This is due mostly to penetration loss of the obstructions between the TX and RX. In fact, when focusing on penetration loss, we found that building walls can inflict penetration losses as high as 40.5 dB for I2I and as high as 66.5 dB for O2I scenarios. In addition, it was found that humans can inflict penetration loss of up to 26 dB at 60 GHz. Also at 60 GHz, the seasonality of trees demonstrated that in summer, when foliage is thickest, the penetration loss was up to 27 dB, but then relaxed to 22 dB in winter. Most interestingly, we reported on the percentage of total received power attributed to diffuse multipath, which was found to be as high as 47%. Finally, we showed that wide-sense stationarity will generally not hold in mmWave small-scale fading due to the sparsity of the channel, the highly directional antennas, and the ultra-wide bandwidths.

References

[1] *Ericsson Mobility Report*, Ericsson, Stockholm, Sweden, Jun 2021. [Online]. Available: https://www.ericsson.com/en/mobility-report

[2] I. A. Hemadeh, K. Satyanarayana, M. El-Hajjar, and L. Hanzo, "Millimeter-wave communications: physical channel models, design considerations, antenna constructions, and link-budget," *IEEE Commun. Surveys & Tutorials*, vol. 20, no. 2, pp. 870-913, Dec. 2017.

[3] M. Shafi *et al*., "5G: A tutorial overview of standards, trials, challenges, deployment, and practice," *IEEE J. Sel. Areas Commun.*, vol. 35, no. 6, pp. 1201–1221, June 2017.

[4] P. B. Papazian, C. Gentile, K. A. Remley, J. Senic, and N. Golmie, "A radio channel sounder for mobile millimeter-wave communications: system implementation and measurement assessment," *IEEE Trans. Microw. Theory and Techniques*, vol. 64, no. 9, pp. 2924-2932, Sept. 2016.

[5] R. Sun, P. B. Papazian, J. Senic, Y. Lo, J.-K. Choi, K.A. Remley, and C. Gentile, "Design and calibration of a double-directional 60 GHz channel sounder for multipath component tracking," *IEEE Euro. Conf. Antennas and Propagation*, Mar. 2017.

[6] Terragraph, Facebook, Menlo Park, California, USA, 2021. [Online]. Available: https://terragraph.com/

[7] H. Friis, "A note on a simple transmission formula," *Proceedings of the IRE*, vol. 34, no. 5, pp. 254-256, May 1964.

[8] J. Senic, C. Gentile, P. B. Papazian, J.-K. Choi, K.A. Remley, and J.-K. Choi, "Analysis of E-band path loss and propagation mechanisms in the indoor environment," *IEEE Trans. Antennas and Propagation*, vol. 65, no. 12, pp. 6562-6573, Dec. 2017.

[9] *5G NR mmWave outdoor and indoor deployment strategy*, Qualcomm, San Diego, CA, USA, May 2019. [Online]. Available: https://www.qualcomm.com/media/documents/files/deploying-5g-nr-mmwave-for-indoor-outdoor.pdf

[10] "Propagation data and prediction methods for the planning of indoor radiocommunication systems and radio local area networks in the frequency range 300 MHz to 450 GHz," International Telecommunication Union, Recommendation ITU-R P.1238-11, Sept. 2021. [Online] Available: https://www.itu.int/rec/R-REC-P.1238

[11] S. Y. Jun, D. Caudill, J. Chuang, P. B. Papazian, A. Bodi, C. Gentile, J. Senic, and N. Golmie, "Penetration loss at 60 GHz for indoor-to-indoor and outdoor-to-indoor mobile scenarios," *IEEE Euro. Conf. Antennas and Propagation*, Mar. 2020.

[12] J. Ryan, G. R. MacCartney, and T. S. Rappaport, "Indoor office wideband penetration loss measurements at 73 GHz", *IEEE Int. Conf. Commun. Wksp.*, May 2017.

[13] H. Zhao *et al*., ''28 GHz millimeter wave cellular communication measurements for reflection and penetration loss in and around buildings in New York City,'' *IEEE Int. Conf. Commun.*, Jun. 2013.

[14] A. Bhardwaj, D. Caudill, C. Gentile, J. Chuang, J. Senic, and D. G. Michelson, "Geometrical-empirical channel propagation model for human presence at 60 GHz," *IEEE Access*, vol. 9, pp. 38467-38478, Mar. 2021.

[15] "Attenuation in vegetation," International Telecommunication Union, Recommendation ITU-R P.833-10, Sept. 2021. [Online] Available: https://www.itu.int/rec/R-REC-P.833/en

[16] C. Lai, R. Sun, C. Gentile, P. B. Papazian, J. Wang, and J. Senic, "Methodology for multipath-component tracking in millimeter-wave channel modeling," *IEEE Trans. Antennas Propag.*, vol. 67, no. 3, pp. 1826-1836, Mar. 2019.

[17] S. Blandino, J. Senic, C. Gentile, D. Caudill, J. Chuang, and A. Kayani, "Markov multi-beamtracking in SU-MIMO with 60 GHz mobile channel measurements," *IEEE Open J. Veh. Technol.*, to be published.

[18] A. Hughes, S. Y. Jun, C. Gentile, D. Caudill, J. Chuang, J. Senic, and D. G. Michelson, "Measuring the impact of beamwidth on the correlation distance of 60 GHz indoor and outdoor channels," *IEEE Open J. Veh. Technol.*, vol. 2, pp. 180-193, Mar. 2021.

[19] D. A. Dickey and W. A. Fuller, "Distribution of the estimators for autoregressive time series with a unit root, " *J. Amer. Statist. Assoc*., vol. 74, no. 366a, pp. 427-431, 1979.